NASA Technical Memorandum 101949

Influence of Thickness and Camber on the Aeroelastic Stability of Supersonic Throughflow Fans: An Engineering Approach

John K. Ramsey
Lewis Research Center
Cleveland, Ohio

(NASA-TM-101949) INFLUENCE OF THICKNESS AND CAMBER ON THE AEROELASTIC STABILITY OF SUPERSONIC THROUGHFLOW FANS: AN ENGINEERING APPROACH (NASA. Lewis Research Center) 22 p CSCL 01A G3/02

N89-25957

Unclas
0219569

June 1989

NASA

INFLUENCE OF THICKNESS AND CAMBER ON THE AEROELASTIC STABILITY OF SUPERSONIC THROUGHFLOW FANS: AN ENGINEERING APPROACH

John K. Ramsey
National Aeronautics and Space Administration
Lewis Research Center
Cleveland, Ohio 44135

E-4642

SUMMARY

An engineering approach was used to include the nonlinear effects of thickness and camber in an analytical aeroelastic analysis of cascades in supersonic axial flow (supersonic leading-edge locus). A hybrid code using Lighthill's nonlinear piston theory and Lane's linear potential theory was developed to include these nonlinear effects. Lighthill's theory was used to calculate the unsteady pressures on the noninterference surface regions of the airfoils in cascade. Lane's theory was used to calculate the unsteady pressures on the remaining interference surface regions. Two airfoil profiles were investigated - a supersonic throughflow fan design and a NACA 66-206 airfoil with a sharp leading edge.

Results show that compared with predictions of Lane's potential theory for flat plates, the inclusion of thickness (with or without camber) may increase or decrease the aeroelastic stability, depending on the airfoil geometry and operating conditions. When thickness effects are included in the aeroelastic analysis, inclusion of camber will influence the predicted stability in proportion to the magnitude of the added camber. The critical interblade phase angle, depending on the airfoil profile and operating conditions, may also be influenced by thickness and camber. Compared with predictions of Lane's linear potential theory, the inclusion of thickness and camber decreased the aerodynamic stiffness and increased the aerodynamic damping at Mach 2 and 2.95 for a cascade of supersonic throughflow fan airfoils oscillating 180° out of phase at a reduced frequency of 0.1.

INTRODUCTION

In recent years, there has been increased interest in providing efficient supersonic propulsion technology for supersonic transport applications. One concept that shows considerable promise is the supersonic throughflow fan (SSTF) engine. A detailed description of this engine and its benefits, as well as associated research, is given in references 1 and 2 and is described briefly here. This engine concept, if successful, will realize a 12-percent improvement in installed specific fuel consumption and a 25-percent reduction in installed weight compared with a nonafterburning turbofan. The SSTF will efficiently process the intake airflow at supersonic throughflow velocities, thereby eliminating the need for a conventional supersonic inlet system. Thus, the inlet weight reduction realized by using the SSTF will be about one-half that of conventional supersonic inlets. Other advantages include fewer fan stages required to achieve a given pressure ratio, less boundary-layer bleed drag, better inlet pressure recovery, and better matching of bypass ratio variations to flight Mach number.

Previous experimental research on the SSTF concept is extremely limited (refs. 3 to 5). Therefore, to evaluate the concept and potential of an SSTF, NASA Lewis Research Center is currently conducting research to design, build, and test an SSTF (refs. 6 and 7). During the original design of the rotor blades, aeroelastic stability became a concern. Consequently a linear, two-dimensional unsteady potential theory presented by Lane (ref. 8) was developed into a computer program (ref. 9) and incorporated into an existing aeroelastic code for use in the aeroelastic stability analysis of the SSTF (ref. 10). The blades were shown to be unstable, and consequently were redesigned. This analysis considered the cascade of blades to be flat plates. In an effort to improve our analysis capabilities, we desired to incorporate the effects of thickness and camber into our aeroelastic model.

Previous analytical work in the area of unsteady supersonic flow in cascades with supersonic leading-edge locus (SLEL) has been limited to flat-plate airfoil geometries (refs. 8 to 18). Currently, there is an effort at NASA Lewis to couple supersonic versions of computational fluid dynamic (CFD) codes (refs. 19 to 21) that include nonlinear thickness and camber effects with a structural dynamic code (time domain) (ref. 22) to computationally solve this problem. However, CFD structural-dynamic tools will probably not be used in the near future for initial aeroelastic calculations. To calculate the flutter point in torsion of the original SSTF with 58 blades, using the CFD structural-dynamic code (ref. 19), a large amount of CPU time would be required on the Cray XMP (personal communication with D. Huff, Dr. D. Hoyniak, and Dr. T.S.R. Reddy of NASA Lewis Research Center). Therefore, CFD structural-dynamic codes will probably be used to refine the flutter boundaries predicted by much more simple and efficient analytical codes.

The dilemma, therefore, is that coupled CFD structural-dynamic codes that include nonlinear thickness and camber effects are computationally lengthy, not presenting themselves as practical flutter analysis tools, whereas the linear analytical codes available, which take much less CPU time, do not include nonlinear thickness and camber effects. Therefore, Lighthill's nonlinear piston theory was utilized as a first attempt to include thickness and camber effects in an analytical aeroelastic stability analysis for cascades with SLEL (personal communication with Dr. J. Adamczyk of NASA Lewis Research Center, Cleveland, OH, and Dr. M.F. Platzer of the Naval Postgraduate School, Monterey, CA). As a result, the aeroelastic stability of cascades with SLEL, including the effects of thickness and camber, can be calculated efficiently. Consequently, the existing unsteady aerodynamic code (ref. 9) was modified to include the nonlinear piston theory.

NONLINEAR PISTON THEORY

Three nonlinear unsteady aerodynamic theories for isolated airfoils are known to the author. They are Van Dyke's theory (ref. 23), Lighthill's nonlinear piston theory (refs. 24 to 27), and Landahl's theory (ref. 28). The simplicity of Lighthill's nonlinear piston theory is evident from references 24 and 25, where it is shown that the analytical expression for the unsteady pressure is a simple function of Mach number and slope of the airfoil surface. In reference 26, figure 8, Ashley compares an experimental flutter point for a wing with various theories - piston theory (zero thickness), piston theory (with thickness), and exact linearized theory (Garrick and Rubinow, ref. 29).

Ashley shows that the piston theory (with thickness) agrees most closely with the experimental flutter point for a Mach number slightly less than 2. Thus because of its simplicity and accuracy with respect to flutter calculations, Lighthill's nonlinear piston theory was used to predict the unsteady pressure distribution in the noninterference surface regions of the airfoils.

A brief review of Lighthill's theory will be described here for the reader's convenience. The normal velocity at any point on the airfoil surface is given by

$$W = U\Theta + w' \tag{1}$$

where Θ is the local steady inclination of the airfoil surface to the free stream, w' is the unsteady component, and Θ is positive for compression waves and negative for expansion waves. Thus for an airfoil in steady state, with upper (+) and lower (-) surfaces given by $f(x)^{(\pm)}$ and unsteady displacement $h = Y(x,t)$, the slope and unsteady downwash for the upper (suction) and lower (pressure) surfaces are

$$\Theta^{(\pm)} = f_x(x)^{(\pm)} \mp \bar{\alpha} \tag{2}$$

$$w'^{(\pm)} = \mp \left(U \frac{\partial}{\partial x} + \frac{\partial}{\partial t}\right) Y(x,t) \tag{3}$$

The steady-state angle of attack $\bar{\alpha}$ is not utilized in the present work.

As presented in reference 24, the pressure on the airfoil surface is given by

$$p = p_\infty \left(1 + \frac{\gamma - 1}{2} \frac{W}{a_\infty}\right)^{2\gamma/\gamma-1} \tag{4}$$

By expanding equation (4) in a binomial series, substituting W in the expansion with equation (1), retaining terms linear in w', and making use of the following relations,

$$p_\infty = \rho_\infty R T_\infty \qquad a_\infty = \sqrt{\gamma R T_\infty} \quad \text{and} \quad U_\infty = M a_\infty$$

the unsteady pressure on the airfoil surface becomes (ref. 27)

$$p'^{(\pm)} = \mp \rho_\infty a_\infty \left[1 + \frac{\gamma + 1}{2} M\Theta + \frac{\gamma + 1}{4} M^2\Theta^2\right] w' \tag{5}$$

The well-known expression for downwash w' is given as

$$w' = U_\infty \left\{ \alpha_s + ik \frac{h_s}{c} + \alpha_s \left(\frac{x}{c} - \frac{x_0}{c}\right) \right\} e^{i\omega t} \tag{6}$$

Substituting w' in equation (5) with equation (6), yields the following equation for the unsteady pressure

$$p'^{(\pm)} = \mp\rho_\infty U_\infty^2\left(\frac{1}{M} + \frac{\gamma+1}{2}\Theta + \frac{\gamma+1}{4}M\Theta^2\right)\left\{\alpha_s + ik\left[\frac{h_s}{c} + \alpha_s\left(\frac{x}{c} - \frac{x_0}{c}\right)e^{i\omega t}\right]\right\} \quad (7)$$

Equation (7) was used to calculate the unsteady pressures on the noninterference surface regions of the airfoils in cascade.

APPROACH

Figure 1 is a schematic of a cascade of airfoils in supersonic axial flow with SLEL. As shown, portions of each airfoil surface are noninterference surfaces: they behave as if each airfoil was isolated from its neighbors. In particular, the unsteady pressure distribution on surface regions 1 and 2 of airfoil B are not influenced by the presence of airfoils A and C. Therefore, the unsteady pressures on surface regions 1 and 2 are not influenced by interblade phase angle. The unsteady pressures on regions 1 and 2 can therefore be calculated by using a nonlinear isolated airfoil theory which includes thickness and camber effects. The unsteady pressure on the remainder of the airfoil (surface regions 3 and 4) can be calculated by using a linear flat-plate theory. The unsteady pressure distribution was generated by these two separate theories. In addition, the oblique shocks were assumed to be Mach lines and to reflect off of the airfoils at the same locations and in the same manner that is predicted by Lane's theory (ref. 8) using flat plates.

LIMITATIONS OF APPROACH

Because of the assumptions Lighthill made in deriving his nonlinear theory (refs. 24 and 25), two limitations must be adhered to when it is used. The first limitation is that the airfoil total normal velocity must be less than the free-stream speed of sound. This limiting condition is given as

$$M\left[\Theta + \frac{\varepsilon}{c}2k\right] < 1$$

in reference 24 (Lighthill considers the theory to still have value as a rough approximation even when the left side is greater than 1). Since ε is assumed to be extremely small for flutter analysis, the limitation is reduced to $M|\Theta| < 1$, which agrees with reference 25.

There is also a limitation on the Mach number range in which Lighthill's nonlinear piston theory is applicable. Miles (ref. 25) states that Lighthill's piston theory can be used for flutter analysis at Mach numbers as low as 2. Morgan et al. (ref. 30) show that biconvex airfoil flutter values calculated by the theories of Van Dyke (ref. 23), Landahl (ref. 28), and Lighthill (ref. 24) show good agreement for $M \geq 2$ to 3. Ashley (ref. 26) shows that Lighthill's nonlinear piston theory correlates well with an experimental flutter point at a Mach number slightly less than 2. Zartarian (ref. 27) recommends Lighthill's piston theory for trend studies and preliminary design purposes even in parameter ranges where it lacks enough quantitative accuracy for precise calculations. Scruton (ref. 31) shows that the aerodynamic stiffness and damping derivatives predicted by Lighthill's nonlinear piston theory are in reasonably good agreement with Van Dyke's theory (ref. 23) at Mach 2.43. The damping derivative predicted by Lighthill's theory also showed good agreement with Van

Dyke's theory at Mach 1.79 for a single wedge airfoil pitching about midchord (ref. 31). In light of this research, a lower bound of Mach 2 was set for this present work.

There are also certain limitations on the analysis because the nonlinear thickness and camber effects are introduced into the analysis in the noninterference surface regions only. For a given cascade geometry and low Mach number, the noninterference surface region of the airfoil is a small portion of the overall chord length. At some greater Mach number, depending on the cascade geometry, the entire airfoil is isolated (the noninterference surface region is the length of the entire chord). For low Mach numbers, the nonlinear portion of the analysis should have little influence on the overall stability calculations. As the Mach number increases, the nonlinear portion of the analysis has more influence.

CODE VERIFICATION

As stated previously, the unsteady aerodynamic code (ref. 9) was modified to include equation (7) for use on the noninterference surface regions of the cascade of airfoils. This modified unsteady aerodynamic code is denoted as code 2. The unsteady aerodynamic code that consists exclusively of Lane's theory (ref. 9) is denoted as code 1. Codes 1 and 2 are identical except for calculation of the pressures in the noninterference surface regions of the airfoils.

Code 2 was verified in several ways. First, to verify the nonlinear portion of the code, the imaginary part of the moment coefficient due to pitching motion for a biconvex airfoil (with $k = 1$) predicted by code 2, was compared with Lighthill's (ref. 24) aerodynamic damping derivatives at Mach 2 with $\tau = 0.05$ and 1, and at Mach 3 with $\tau = 0.03$ and 1. In all cases the difference was less than 1.59 percent.

Second, to verify that the piston theory subroutine was interacting properly in the existing code (ref. 9), the moment coefficient and the unsteady pressure distributions due to pitching motion for a cascade of flat plates predicted by code 2 were compared with those predicted by code 1 by setting $\Theta = 0$ in code 2. The cascade parameters used are shown in table I. Setting $\Theta = 0$ in code 2 reduces Lighthill's nonlinear piston theory to linear piston theory. Linear piston theory is not expected to agree closely with linear potential theory in the Mach number range ($2 \leq M \leq 3$) used in this comparison. However general trends should still be similar. As shown in figures 2 to 6, the general trends in the moment coefficient and unsteady pressures are similar, validating that the piston theory subroutine is interacting properly within the code.

STRUCTURAL MODEL

The classical typical section, as shown in figure 7, was used to model the structure. Each airfoil is assumed to be a two-dimensional oscillator supported by bending and torsional springs. The airfoil is assumed to be rigid in the chordwise direction. Coupling between bending and torsional motion is

modeled through the offset distance between the center of gravity and the "elastic axis."

EQUATIONS OF MOTION

The equations of motion used (which are presented in ref. 32) are

$$\begin{bmatrix} m_s & S_{\alpha s} \\ S_{\alpha s} & I_{\alpha s} \end{bmatrix} \begin{Bmatrix} \frac{d^2}{dt^2}\left(h_s e^{i\omega t}\right) \\ \frac{d^2}{dt^2}\left(\alpha_s e^{i\omega t}\right) \end{Bmatrix} + \begin{bmatrix} 1 + 2i\zeta_{hs}\, m_s \omega_{hs}^2 & 0 \\ 0 & \left(1 + 2i\zeta_{\alpha s}\right) I_{\alpha s} \omega_{\alpha s}^2 \end{bmatrix} \times \begin{Bmatrix} h_s e^{i\omega t} \\ \alpha_s e^{i\omega t} \end{Bmatrix} = \begin{Bmatrix} -L_s \\ M_s \end{Bmatrix} \tag{8}$$

The parameters L_s and M_s are the aerodynamic lift and moment, respectively, expressed in terms of nondimensional coefficients as

$$L_s = \pi\rho b^3 \omega^2 \sum_{r=0}^{N-1} \left[l_{hhr} \frac{h_{ar}}{b} + l_{h\alpha r} \alpha_{ar} \right] e^{i(\omega t + \beta_r s)} \tag{9}$$

$$M_s = -\pi\rho b^4 \omega^2 \sum_{r=0}^{N-1} \left[l_{\alpha hr} \frac{h_{ar}}{b} + l_{\alpha\alpha r} \alpha_{ar} \right] e^{i(\omega t + \beta_r s)} \tag{10}$$

where the coefficients l_{hhr}, $l_{h\alpha r}$, $l_{\alpha hr}$, and $l_{\alpha\alpha r}$ are calculated by Lighthill's nonlinear piston theory and Lane's linear potential theory for given values of M, k, c/g, ξ, β_r, and a_e. For the sake of completeness, equations (9) and (10) allow for structurally mistuned blades in cascade even though a mistuned cascade was not studied in this work. The aeroelastic stability of the system is determined by solving a complex eigenvalue problem, resulting from an equation (8) written for each blade. For this research, the hybrid unsteady aerodynamic code consisting of Lighthill's nonlinear piston theory and Lane's linear potential theory was incorporated into an existing Lewis code, MISER2 (contact COSMIC, The University of Georgia, Athens, GA 30602 concerning the availability of MISER2) (ref. 32), which solves this complex eigenvalue problem.

BLADE PARAMETERS

Table I lists the various cascade parameters which were used for the aeroelastic analysis. These values are for the 73.3 percent span location of the original SSTF design. In order to study the effects of thickness and camber

on the aeroelastic stability of an SSTF, an airfoil camber and thickness distribution must be chosen. The geometries used in the aeroelastic stability analysis were a flat plate, variations of a NACA 66-206 airfoil (ref. 33), and variations of the original SSTF airfoil. These airfoil profiles are shown in figures 8 to 10. The camber lines of the original SSTF and NACA airfoils are compared in figure 11. The surface slopes of the NACA 66-206 and the original SSTF airfoil section were within the necessary criteria ($M|\Theta| < 1$) previously mentioned. Unlike the profile given in reference 35, the NACA profile was modified to have a sharp leading edge. The cascade parameters were held constant for all of the airfoil profiles.

As already stated, the slopes of the suction and pressure airfoil surfaces are needed to compute the unsteady pressure on the noninterference surface regions. A five-degree power series was fit to the coordinates of the suction and pressure surfaces of the NACA 66-206 as well as to the original SSTF airfoil. The resulting equations $f(x)^{(\pm)}$ were differentiated to give the slopes ($f_x(x)^{(\pm)} = \Theta$) of the suction and pressure surfaces as a function of chord location. The power series coefficients for the slopes of the NACA 66-206 profile with and without camber are shown in table II. The equations for the slopes were input to the aeroelastic code for use by the piston theory subroutine.

RESULTS

The cascade consisting of the original 58 supersonic throughflow airfoils will be designated from here on as SSTF. The original SSTF airfoil profile is shown in figure 10. The cascade consisting of the 10 NACA 66-206 airfoils will be designated from here on as the NACA cascade. Its airfoil profile is shown in figure 8. Only 10 blades were chosen for the NACA cascade to reduce computational effort.

As stated previously, the nonlinear portion of the code has more influence on the analysis as the Mach number increases. This is due to the fact that the noninterference surface regions of the airfoils, as shown in figure 1, increase with increasing Mach number. At Mach 2, the noninterference surface region is approximately 60 and 30 percent of the suction and pressure surfaces, respectively. At Mach 3, the noninterference surface region is approximately 90 and 60 percent of the suction and pressure surfaces, respectively. Therefore it can be concluded that for this study, the nonlinear portion of the code has a significant influence on the aeroelastic analysis. Indeed at Mach 3, almost the entire unsteady pressure on the suction surface is calculated by nonlinear piston theory.

Figures 3 to 6 show the unsteady pressure distributions for torsional motion about midchord of the SSTF at Mach 2 and 2.95 for a reduced frequency k of 0.1 and an interblade phase angle of 180°. Only the portion of the pressure plots associated with the noninterference surface regions of the airfoils are shown since the remaining pressure distribution is that predicted by Lane's potential theory. Up to the first shock reflection both upper and lower unsteady surface pressures are calculated using Lighthill's nonlinear piston theory. Between the first and second shock reflection, the unsteady pressure on the suction and pressure surfaces are calculated by nonlinear piston theory

and potential theory, respectively. These plots are discussed in the following sections.

The flutter boundaries for torsional instability of the NACA cascade are shown in figure 12. The flutter boundaries for torsional instability of the original SSTF are shown in figure 13. Plots of critical interblade phase angle versus relative Mach number for the NACA cascade and SSTF are presented in figures 14 and 15. These plots are discussed in the following sections.

Thickness Effects

Figure 9 shows that the thickness distribution for the NACA airfoil is larger than that for the original SSTF airfoil. Upon integration of the unsteady pressure distribution in figures 3 to 6, for the SSTF, it was found that thickness decreased the aerodynamic stiffness and increased the aerodynamic damping (although still negative) as compared with that predicted by Lane's potential theory for a flat-plate profile. This trend held true at Mach 2 and 2.95 for a reduced frequency of 0.1.

As shown in figure 12, the inclusion of thickness (symmetrical profile) in the aeroelastic stability analysis increased the stability for the NACA cascade compared with the analysis using Lane's potential theory for flat plates. The thickness distribution had more influence on the aeroelastic stability than did the camber, when compared with the flat-plate analysis. Compared with an analysis using Lane's theory for flat plates, the inclusion of thickness (symmetrical profile) decreased the stability of the SSTF for $2 \leq M$ and less than approximately 2.3, and increased the stability above an approximate Mach number of 2.3.

Camber Effects

As shown in figure 11, the camber of the original SSTF airfoil is much greater than that of the NACA airfoil. Upon integration of the unsteady pressure distribution in figures 3 to 6, for the SSTF cascade, it was found that adding camber to the thickness (symmetrical) distribution of the SSTF further decreased the aerodynamic stiffness and further increased the aerodynamic damping (although still negative) compared with the symmetrical profile. These trends held true at Mach 2 and 2.95 for a reduced frequency of 0.1.

From figure 12 it is shown that the inclusion or exclusion of camber in the aeroelastic stability analysis of the NACA cascade, when thickness is included, has little effect on stability. This is not surprising since the camber of the NACA profile is small. However, as shown in figure 13, the inclusion or exclusion of camber in the aeroelastic stability analysis for the SSTF, when thickness is included, has a larger effect on stability as compared with the NACA cascade. This is also not surprising since the SSTF airfoil has more camber than the NACA airfoil. Including camber with thickness increased the predicted stability for the SSTF for Mach numbers slightly above 2.0 with respect to the analysis using Lane's theory for flat plates. The inclusion of camber with thickness also increased the stability of the SSTF when compared with the analysis with thickness only.

Interblade Phase Angle

As shown in figure 14, the aeroelastic analysis of the NACA cascade, including thickness with and without camber, predicted a critical interblade phase angle of 216° from Mach 2 to 2.2. From Mach 2.3 to 3.0 the predicted critical interblade phase angle was 180°. The flat-plate analysis using Lane's theory predicted the same results except at Mach 2.3. Here the aeroelastic analysis using the flat plate predicted a critical interblade phase angle of 216° as opposed to the aeroelastic analysis including thickness with or without camber, which predicted a critical interblade phase angle of 180°.

As shown in figure 15, the aeroelastic analysis including thickness with or without camber predicted that the critical interblade phase angle of the SSTF would decrease from 204.8° at Mach 2, to 180° at Mach 2.95. This is similar to the trend presented in reference 10. The aeroelastic analysis using flat plates predicted the same trend, except at Mach 2.7. Here the aeroelastic analysis with thickness and camber resulted in a critical interblade phase angle of 186.2° as opposed to 180° from the analysis using flat plates and thickness only (symmetrical).

CONCLUSIONS

As a means of determining the influence of thickness and camber on the aeroelastic stability of supersonic throughflow fans, Lighthill's nonlinear piston theory, which includes thickness and camber effects, and Lane's linear potential theory have been developed into a hybrid unsteady aerodynamic code. This hybrid code, coupled with an existing aeroelastic code has been applied to a cascade of NACA 66-206 airfoils (NACA cascade) and a cascade consisting of the original supersonic throughflow fan airfoils (SSTF) in supersonic axial flow with supersonic leading-edge locus. Through this engineering approach, the effects of thickness and camber on the aeroelastic stability of supersonic throughflow fans have been investigated.

The major conclusions from this investigation follow:

1. Depending on airfoil geometry and operating conditions, the inclusion of thickness with or without camber may either increase or decrease the predicted aeroelastic stability when compared with an analysis using Lane's potential theory for flat plates.

2. When thickness effects are included in the aeroelastic analysis, inclusion of camber will influence the predicted stability in proportion to the magnitude of the added camber.

3. The critical interblade phase angle, depending on the airfoil profile and operating conditions, may be influenced by thickness and camber.

4. Thickness decreased the aerodynamic stiffness and increased the aerodynamic damping at Mach 2 and 2.95 for the SSTF oscillating 180° out of phase at a reduced frequency of 0.1, when compared with Lane's potential theory for flat plates.

5. The inclusion of camber when thickness is present served to further decrease the aerodynamic stiffness and increase the aerodynamic damping at Mach 2 and 2.95 for the SSTF at the previously mentioned interblade phase angle and reduced frequency.

ACKNOWLEDGMENTS

The author wishes to express his gratitude to Dr. John Adamczyk of NASA Lewis and Dr. M.F. Platzer of the Naval Postgraduate School, Monterey, California, whose ideas of using piston theory have made this paper possible.

APPENDIX - SYMBOLS

A	coefficients in power series describing airfoil surface slope
a_e	elastic axis position
a_∞	free-stream speed of sound
b	half-chord
c	chord
$f(x)^{(\pm)}$	function describing steady-state upper suction (+) and lower pressure (-) airfoil surfaces, positive away from airfoil on each side of it
g	circumferential gap between adjacent blades
h_{ar}	plunging amplitude in r^{th} aerodynamic mode
h_s	plunging amplitude of the s^{th} blade
$I_{\alpha s}$	polar moment of inertia about elastic axis of s^{th} blade
i	imaginary unit
k	reduced frequency, $\omega b/U_\infty$
k_{hs}	bending stiffness of s^{th} blade
$k_{\alpha s}$	torsional stiffness of s^{th} blade
L_s	aerodynamic lift of s^{th} blade
$l_{hhr}, l_{h\alpha r}$	nondimensional lift coefficients in r^{th} aerodynamic mode due to plunging and pitching motions, respectively
$l_{\alpha hr}, l_{\alpha\alpha r}$	nondimensional moment coefficients in r^{th} aerodynamic mode due to plunging and pitching motions, respectively
M	relative Mach number
M_s	aerodynamic moment of s^{th} blade
m_s	mass per unit span of s^{th} blade
N	number of blades
p	pressure on airfoil surface
p'	unsteady pressure on airfoil surface
$p'^{(\pm)}$	unsteady pressure on the upper (+) and lower (-) airfoil surface, respectively

p_∞	free-stream static pressure
R	specific gas constant
r	integer specifying aerodynamic mode
$r_{\alpha s}$	nondimensional radius of gyration of s^{th} blade
$S_{\alpha s}$	mass moment about elastic axis ($mbx_{\alpha s}$) of s^{th} blade
T_∞	free-stream static temperature
t	time
U_∞	free-stream air velocity relative to blade
W	total normal velocity
w'	unsteady normal velocity (downwash)
x	streamwise coordinate
$x_{\alpha s}$	nondimensional static unbalance of s^{th} blade
x_0	streamwise coordinate of pitching axis referenced from the airfoil leading edge, $x_0 = b + a_e b$
Y	transverse coordinate
$\bar{\alpha}$	steady-state angle of attack
α_{ar}	pitching amplitude in r^{th} aerodynamic mode
α_s	pitching amplitude of s^{th} blade
β_r	interblade phase angle of r^{th} aerodynamic mode
γ	ratio of specific heats (assume = 1.4)
ε	maximum displacement in airfoil oscillation
$\theta^{(\pm)}$	slope of airfoil surface (positive for compression waves, negative for expansion waves) on upper suction surface (+) and lower pressure surface (-)
μ	mass ratio, $m_s/\pi\rho_\infty b^2$
ξ	stagger angle
ρ_∞	free-stream air density
τ	thickness-to-chord ratio for biconvex airfoil
ω	circular frequency

ω_{hs} bending frequency of s^{th} blade

$\omega_{\alpha s}$ torsional frequency of s^{th} blade

ζ_{hs} critical damping ratio for bending mode of s^{th} blade

$\zeta_{\alpha s}$ critical damping ratio for torsional mode of s^{th} blade

REFERENCES

1. Franciscus, L.C.: The Supersonic Throughflow Turbofan for High Mach Propulsion. NASA TM-100114, 1987 (AIAA Paper 87-2050).

2. Aèropropulsion '87. Session 6: High-Speed Propulsion Technology. NASA CP-10003, 1987.

3. Klapproth, J.F.: A Review of Supersonic Compressor Development. J. Eng. Power, vol. 83, no. 3, July 1961, pp. 258-268.

4. Savage, M.; Boxer, E.; and Erwin, J.R.: Resume of Compressor Research at the NACA Langley Laboratory. J. Eng. Power, vol. 83, no. 2, July 1961, pp. 269-285.

5. Breugelmans, F.A.E.: The Supersonic Axial Component in a Compressor. ASME Paper 75-GT-26, Mar. 1975.

6. Schmidt, J.F., et al.: Supersonic Through-Flow Fan Design. AIAA Paper 87-1746, 1987 (NASA TM-88908).

7. Wood, J.R., et al.: Application of Advanced Computational Codes in the Design of an Experiment for a Supersonic Throughflow Fan Rotor. ASME Paper 87-GT-160, 1987 (NASA TM-88915).

8. Lane, F.: Supersonic Flow Past an Oscillating Cascade With Supersonic Leading-Edge Locus. J. Aeronaut. Sci., vol. 24, no. 1, Jan. 1957, pp. 65-66.

9. Ramsey, J.K.; and Kielb, R.E.: A Computer Program for Calculating Unsteady Aerodynamic Coefficients for Cascades in Supersonic Axial Flow. NASA TM-100204, 1987.

10. Kielb, R.E.; and Ramsey, J.K.: Flutter of a Fan Blade in Supersonic Axial Flow. ASME Paper 88-GT-78, 1988.

11. Miles, J.W.: The Compressible Flow Past an Oscillating Airfoil in a Wind Tunnel. J. Aeronaut. Sci., vol. 23, no. 7, July 1956, pp. 671-678.

12. Drake, D.G.: The Oscillating Two-Dimensional Aerofoil Between Porous Walls. Aeronaut. Q., vol. 8, no. 3, Aug. 1957, pp. 226-239.

13. Gorelov, D.N.: Lattice of Plates in an Unsteady Supersonic Flow. Fluid Dynamics (Engl. Transl.), vol. 1, no. 4, July-Aug. 1966, pp. 34-39.

14. Platzer, M.F.; and Chalkley, H.G.: Theoretical Investigation of Supersonic Cascade Flutter and Related Interference Problems. AIAA Paper 72-377, 1972.

15. Chalkley, H.G.: A Study of Supersonic Flutter. Naval Postgraduate School, Monterey, CA, 1972 (AD-745838).

16. Nagashima, T.; and Whitehead, D.S.: Linearized Supersonic Unsteady Flow in Cascades. ARC-R/M-3811, 1978.

17. Nishiyama, T.; and Kikuchi, M.: Theoretical Analysis for Unsteady Characteristics of Oscillating Cascade Aerofoils in Supersonic Flows. Technol. Rep. Tohoku Univ. (Japan), vol. 38, no. 2, 1973, pp. 565-597.

18. Caruthers, J.E.: Theoretical Analysis of Unsteady Supersonic Flow Around Harmonically Oscillating Turbofan Cascades. Ph.D. Thesis, Georgia Institute of Technology, 1976.

19. Huff, D.L.: Numerical Analysis of Flow Through Oscillating Cascade Sections. AIAA Paper 89-0437, 1989 (NASA TM-101417).

20. Whitfield, D.L., et al.: Three-Dimensional Unsteady Euler Solutions for Propfans and Counter-Rotating Propfans in Transonic Flow. AIAA Paper 87-1197, 1987.

21. Kao, Y.F.: A Two-Dimensional Unsteady Analysis For Transonic and Supersonic Cascade Flows. Ph.D. Thesis, Purdue University, May 1989.

22. Reddy, T.S.R.; Srivastava, R.; and Kaza, K.R.V.: The Effects of Rotational Flow, Viscosity, Thickness, and Shape on Transonic Flutter Dip Phenomena. In: Structures, Structural Dynamics and Materials Conf., 29th, Vol. 2, pp. 1096-1108, 1988 (NASA TM-100811).

23. Van Dyke, M.D.: Supersonic Flow Past Oscillating Airfoils Including Nonlinear Thickness Effects. NACA TN-2982, 1953.

24. Lighthill, M.J.: Oscillating Airfoils at High Mach Number. J. Aeronaut. Sci., vol. 20, no. 6, June 1953, pp. 402-406.

25. Miles, J.W.: Unsteady Flow at Hypersonic Speeds. In: Hypersonic Flow (Proceedings of the Eleventh Symposium of the Colston Research Society held in the University of Bristol), A.R. Collar and J. Tinkler, eds., 1960, Academic Press Inc., pp. 185-197.

26. Ashley, H.; and Zartarian, G.: Piston Theory - A New Aerodynamic Tool for the Aeroelastician. J. Aeronaut. Sci., vol. 23, no. 12, Dec. 1956, pp. 1109-1118.

27. Zartarian, G.; Heller, A.; and Ashley, H.: Application of Piston Theory to Certain Elementary Aeroelastic Problems. Proceedings of the Fourth Midwestern Conference on Fluid Mechanics, Purdue University, 1955, pp. 163-181.

28. Landahl, M.T.: Unsteady Flow Around Thin Wings at High Mach Numbers. J. Aeronaut. Sci., vol. 24, no. 1, Jan. 1957, pp. 33-38.

29. Garrick, I.E.; and Rubinow, S.I.: Flutter and Oscillating Air Force Calculations for an Airfoil in a Two-Dimensional Supersonic Flow. NACA TR-1158, 1946.

30. Morgan, H.G.; Runyan, H.L.; and Huckel, V.: Theoretical Considerations of Flutter at High Mach Numbers. J. Aeronaut. Sci., vol. 25, no. 6, June 1958, pp. 371-381.

31. Scruton, C., et al.: Measurement of Pitching-Moment Derivatives for Aero-Foils Oscillating in Two-Dimensional Supersonic Flow. R&M No. 3234, British A.R.C., 1959.

32. Kaza, K.R.V.; and Kielb, R.E.: Flutter and Response of a Mistuned Cascade in Incompressible Flow. AIAA J., vol. 20, no. 8, Aug. 1982, pp. 1120-1127.

33. Abbott, I.H.; and Von Doenhoff, A.E.: Theory of Wing Sections, Including a Summary of Airfoil Data. Dover Publications Inc., 1959, p. 441.

TABLE I. - CASCADE PARAMETERS

Parameter	SSTF	NACA
Number of blades, N	58	10
Mass ratio, μ	456.2	456.2
Nondimensional radius of gyration of s^{th} blade, $r_{\alpha s}$	0.431	0.431
Stagger angle, ξ	28	28
Ratio of circumferential gap between adjacent blades to chord	0.311	0.311
Ratio of bending frequency to torsional frequency, $\omega_{hs}/\omega_{\alpha s}$	0.5668	0.5668
Elastic axis position, a_e	0	0
Nondimensional static unbalance of s^{th} blade, $x_{\alpha s}$	0	0

TABLE II. - SERIES REPRESENTATION OF NACA PROFILES

$$\theta = \sum_{i=1}^{5} A_i X^{i-1}$$

$$0 \leq X \leq 1$$

Coefficient	Thickness and camber		Symmetrical
	θ^+	θ^-	$\theta^+ (= \theta^-)$
A1	0.27124	0.15037	0.210805
A2	-1.86248	-1.32054	-1.591510
A3	5.59980	4.66200	5.130900
A4	-7.82200	-7.11520	-7.468600
A5	3.72870	3.65935	3.694025

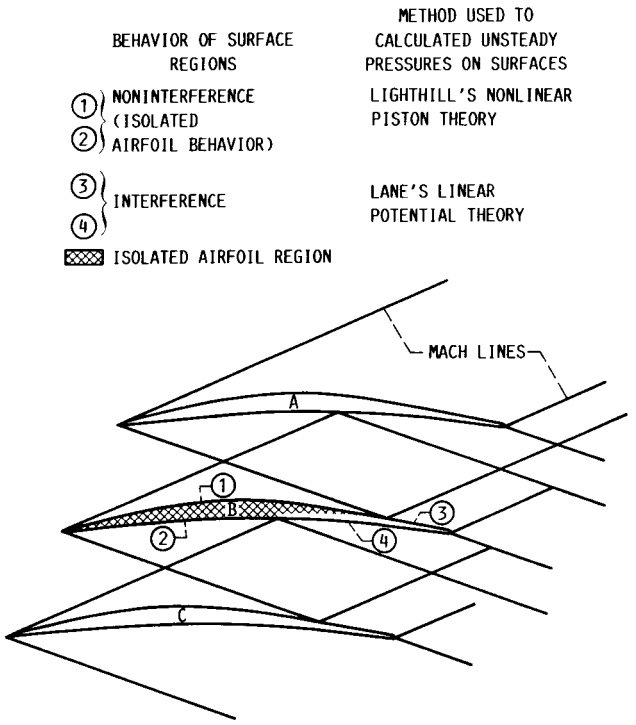

FIGURE 1. - CASCADE IN SUPERSONIC AXIAL FLOW.

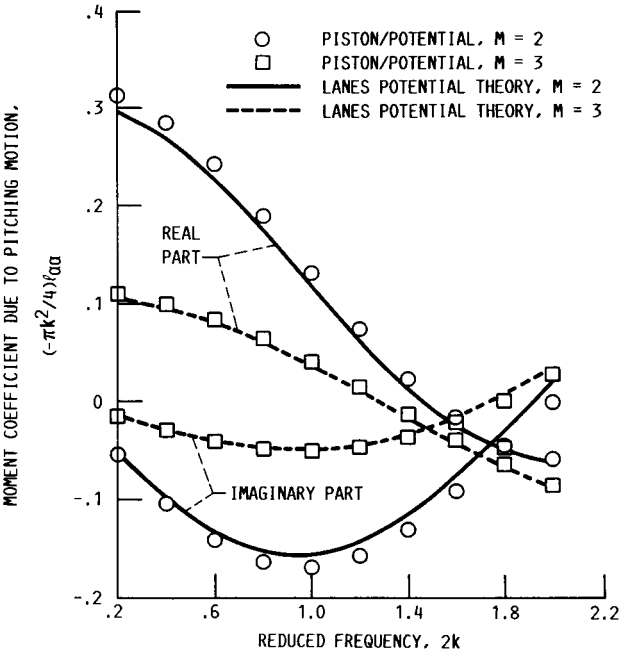

FIGURE 2. - MOMENT COEFFICIENTS DUE TO PITCHING MOTION ABOUT MIDCHORD FOR THE SSTF (FLAT-PLATE CASCADE) WITH INTERBLADE PHASE ANGLE OF 180^0.

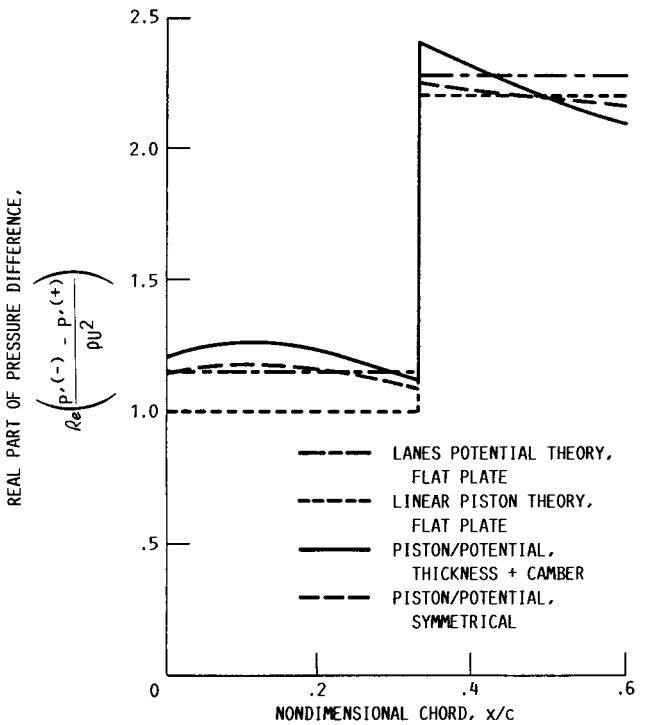

FIGURE 3. - REAL PART OF PRESSURE DIFFERENCE FOR THE SSTF AT MACH 2; REDUCED FREQUENCY, k, 0.1; AND INTERBLADE PHASE ANGLE, 180^0.

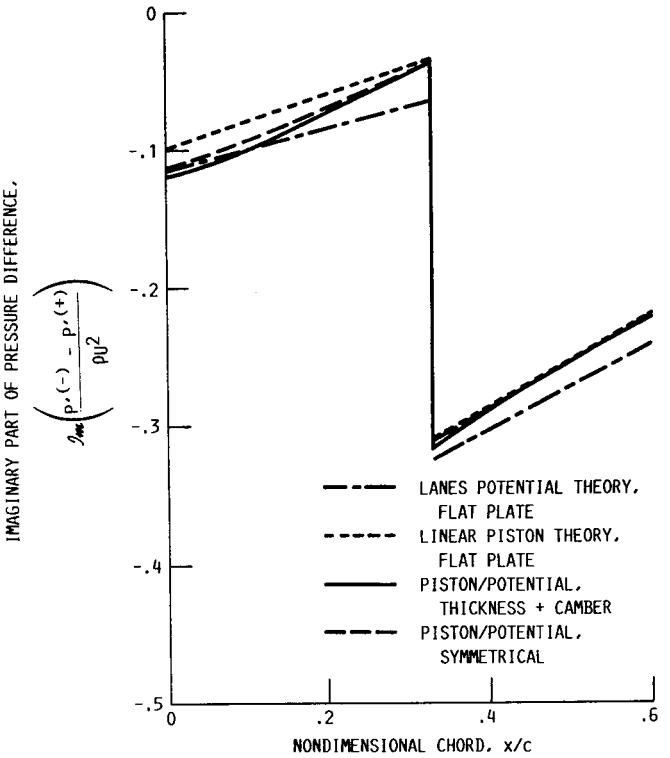

FIGURE 4. - IMAGINARY PART OF PRESSURE DIFFERENCE FOR THE SSTF AT MACH 2; REDUCED FREQUENCY, k, 0.1; AND INTERBLADE PHASE ANGLE, 180^0.

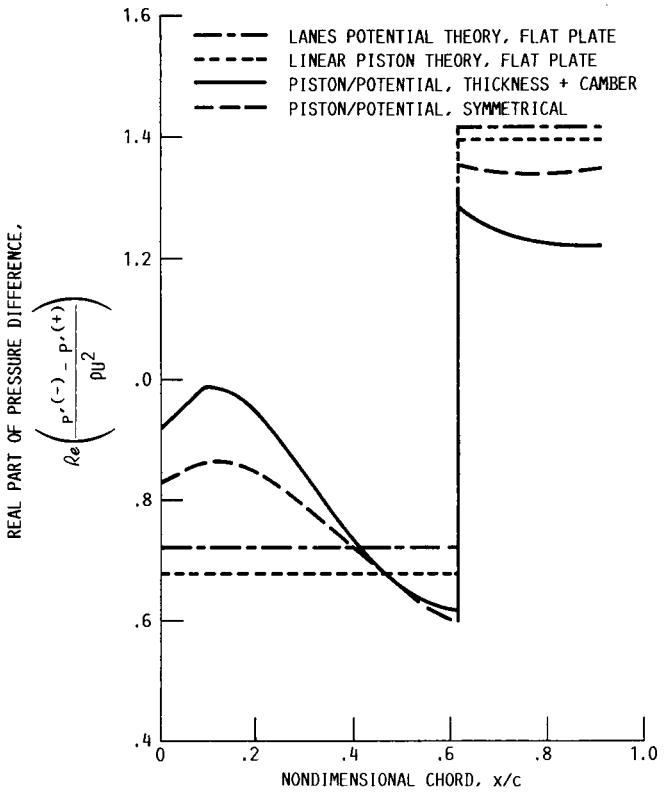

FIGURE 5. - REAL PART OF PRESSURE DIFFERENCE FOR THE SSTF AT MACH 2.95; REDUCED FREQUENCY, k, 0.1; AND INTERBLADE PHASE ANGLE, 180°.

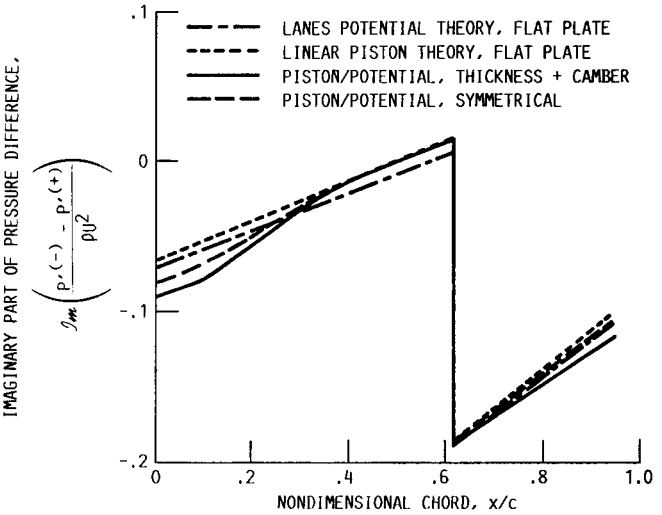

FIGURE 6. - IMAGINARY PART OF PRESSURE DIFFERENCE FOR THE SSTF AT MACH 2.95; REDUCED FREQUENCY, k, 0.1; AND INTERBLADE PHASE ANGLE, 180°.

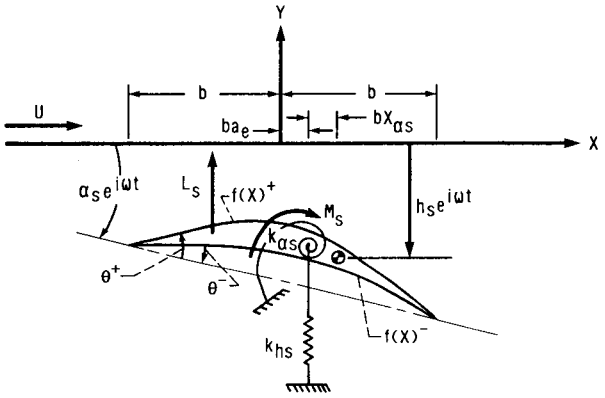

FIGURE 7. - TYPICAL SECTION.

FIGURE 8. - NACA 66-206 AIRFOIL PROFILE.

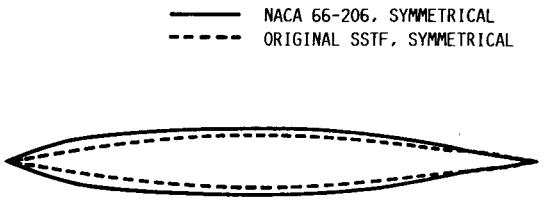

FIGURE 9. - COMPARISON OF NACA 66-206 AND THE ORIGINAL SSTF THICKNESS (SYMMETRIC PROFILE) DISTRIBUTIONS.

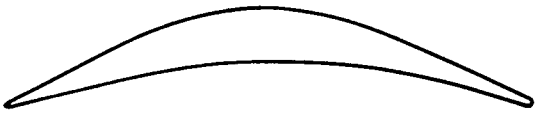

FIGURE 10. - SSTF AIRFOIL PROFILE.

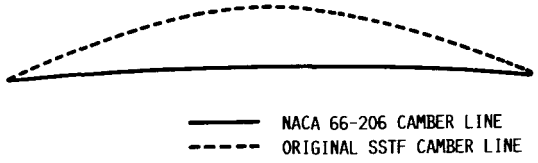

FIGURE 11. - COMPARISON OF NACA 66-206 AND SSTF CAMBER LINES.

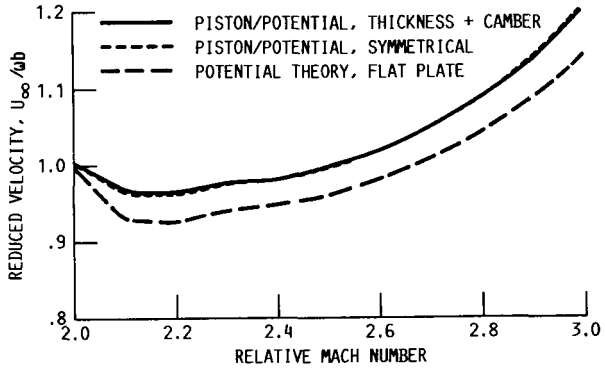

FIGURE 12. - TORSIONAL MODE FLUTTER BOUNDARY FOR THE NACA CASCADE.

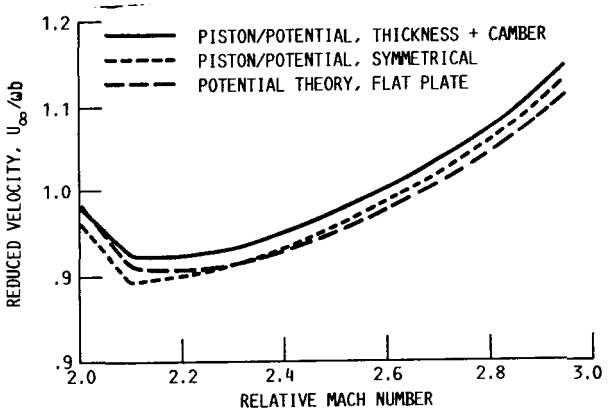

FIGURE 13. - TORSIONAL MODE FLUTTER BOUNDARY FOR THE SSTF.

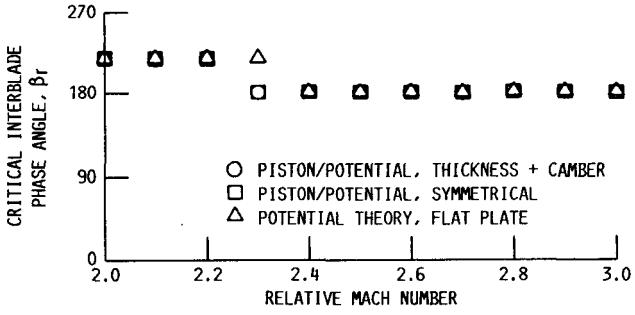

FIGURE 14. - CRITICAL INTERBLADE PHASE ANGLE AS A FUNCTION OF MACH NUMBER FOR THE TORSIONAL MODE FLUTTER OF THE NACA CASCADE.

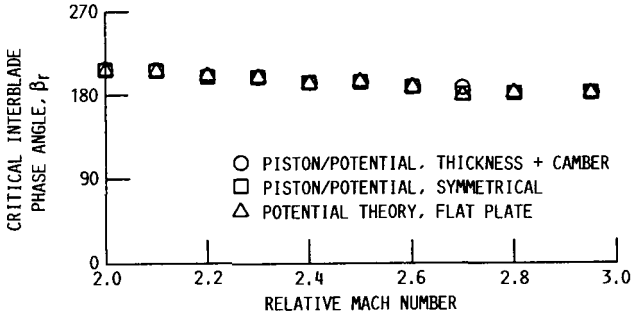

FIGURE 15. - CRITICAL INTERBLADE PHASE ANGLE AS A FUNCTION OF MACH NUMBER FOR THE TORSIONAL MODE FLUTTER OF THE SSTF.

NASA
National Aeronautics and Space Administration

Report Documentation Page

1. Report No.	2. Government Accession No.	3. Recipient's Catalog No.
NASA TM-101949		

4. Title and Subtitle	5. Report Date
Influence of Thickness and Camber on the Aeroelastic Stability of Supersonic Throughflow Fans: An Engineering Approach	June 1989
	6. Performing Organization Code

7. Author(s)	8. Performing Organization Report No.
John K. Ramsey	E-4642
	10. Work Unit No.
	505-63-1B

9. Performing Organization Name and Address	11. Contract or Grant No.
National Aeronautics and Space Administration Lewis Research Center Cleveland, Ohio 44135-3191	
	13. Type of Report and Period Covered
12. Sponsoring Agency Name and Address	Technical Memorandum
National Aeronautics and Space Administration Washington, D.C. 20546-0001	14. Sponsoring Agency Code

15. Supplementary Notes

16. Abstract

An engineering approach was used to include the nonlinear effects of thickness and camber in an analytical aeroelastic analysis of cascades in supersonic axial flow (supersonic leading-edge locus). A hybrid code using Lighthill's nonlinear piston theory and Lane's linear potential theory was developed to include these nonlinear effects. Lighthill's theory was used to calculate the unsteady pressures on the noninterference surface regions of the airfoils in cascade. Lane's theory was used to calculate the unsteady pressures on the remaining interference surface regions. Two airfoil profiles were investigated—a supersonic throughflow fan design and a NACA 66-206 airfoil with a sharp leading edge. Results show that compared with predictions of Lane's potential theory for flat plates, the inclusion of thickness (with or without camber) may increase or decrease the aeroelastic stability, depending on the airfoil geometry and operating conditions. When thickness effects are included in the aeroelastic analysis, inclusion of camber will influence the predicted stability in proportion to the magnitude of the added camber. The critical interblade phase angle, depending on the airfoil profile and operating conditions, may also be influenced by thickness and camber. Compared with predictions of Lane's linear potential theory, the inclusion of thickness and camber decreased the aerodynamic stiffness and increased the aerodynamic damping at Mach 2 and 2.95 for a cascade of supersonic throughflow fan airfoils oscillating 180° out of phase at a reduced frequency of 0.1.

17. Key Words (Suggested by Author(s))	18. Distribution Statement
Supersonic axial flow; Supersonic leading edge locus; Flutter; Cascades; Piston theory; Nonlinear unsteady aerodynamics	Unclassified – Unlimited Subject Category 02

19. Security Classif. (of this report)	20. Security Classif. (of this page)	21. No of pages	22. Price*
Unclassified	Unclassified	22	A03

*For sale by the National Technical Information Service, Springfield, Virginia 22161